Journal of Contemporary Technology and Applied Engineering (JCTAE)

Home Page: https://jctae.journals.ekb.eg/
Published by: Faculty of Engineering, Kafrelsheikh University

Volume: 3 Issue: 2 Year: 2025 Pages: 63 – 81
DOI: 10.21608/jctae.2025.360608.1042
Print ISSN: 2812-5797
Online ISSN: 2812-5800

# NUMERICAL PARAMETRIC STUDY FOR OPTIMAL DESIGN OF DISCONNECTED PILED RAFT FOUNDATION

Received: 14-02-2025
Accepted: 21-02-2025

Ahmed M. Abdel Galil [a,*], Ahmed A. Elsobky [a], Abdel-Fattah A. Youssef [a]

[a] *Civil Engineering Department, Faculty of Engineering, Menoufia University, Menoufia, Egypt.*

[*] Corresponding author: A. M. Abdel Galil ahmed.abdaljalil@sh-eng.menofia.edu.eg

**ABSTRACT.** Disconnected piled raft (DPR) foundation is an innovative solution for sites with poor soil conditions where a conventional raft foundation may not provide a suitable foundation system. In the DPR system, the raft's efficiency is enhanced by incorporating a limited number of disconnected piles, which primarily serve as settlement-reducing elements. A flexible cushion layer is inserted between the raft and the piles to create more uniform stress distribution under the raft. In this research, the performance of the DPR foundation on loose sand soil subjected to vertical loading is investigated through a comprehensive parametric study. 3D finite element analyses employing PLAXIS software are utilized to model the complex interactions within the DPR foundation. The piles and raft are represented as volume elements. The soil response is simulated with the Hardening Soil (HS) approach, which accurately captures the nonlinear elasto-plastic response and the stress-dependent stiffness of the soil. The study examines the effects of cushion thickness, cushion elastic modulus, pile length, and pile diameter on the load-settlement behavior of the DPR foundation, load sharing between the raft and the piles, as well as the axial loads and bending moments experienced by the floating disconnected piles. The findings from this study could be helpful in providing guidelines to achieve the optimal design of the DPR foundation resting on loose sand.

**KEYWORDS:** Disconnected piled raft; Cushion; Parametric study; Three-dimensional finite element; Complex interactions.

## 1. INTRODUCTION

Piled rafts serve as a reliable foundation for constructions built on poor soils because of their ability to efficiently control both total and differential settlements and improve bearing capacity. In piled raft (PR) foundations, the external loads are carried by both the piles and the raft, in contrast to the classic design of pile foundations which assumes that the piles support the entire load, neglecting the raft's bearing capacity [1-5].

Employing piles as settlement reducers in PR foundations offers an economical foundation by reducing the number of piles while fully utilizing their bearing capacity [6-11]. However, when this limited number of piles is structurally integrated with the raft, it can lead to significant bending moments and concentrated axial stresses at the pile heads. Consequently, the load-carrying capacity of the pile could be controlled by its structural strength instead of its geotechnical capacity [12-13]. To minimize the constraint reactions among the raft and the pile heads, [14] proposed a novel foundation system commonly called disconnected piled raft (DPR). In this system, a compacted granular layer is used to separate the piles from the raft. The disconnected piles are not considered structural elements, but rather reinforcement for the subsoil to improve its performance.

Since the development of this novel foundation system, several numerical and experimental studies have been carried out in recent decades to explore the behavior of DPR foundations [15-31]. These studies have focused on principal features such as load sharing ratios, the load transfer mechanism, and the structural response of the disconnected piles. The main findings of these studies have highlighted the important role of the granular cushion in optimizing the stress distribution between the piles and underlying soil and preventing localized structural failure. Moreover, both the geotechnical and geometrical characteristics of the cushion have a profound impact on the DPR foundation. An essential insight from previous research is that the load transfer mechanisms in the DPR system differ fundamentally from those in the PR system, as illustrated in Fig. 1.

For the PR foundation, Fig. 1a demonstrates that at the ground surface, the pile heads, raft, and topsoil beneath the raft undergo identical settlement, as the piles are structurally fixed to the raft. This results in no relative movement between the piles and the surrounding subsoil, i.e., $w_r = w_s = w_p$ where ($w_r$) is the raft's settlement, ($w_s$) is the settlement of the subsoil under the raft between the piles, and ($w_p$) is the settlement of the pile. Therefore, no skin friction is generated, and the neutral plane of the PR system aligns with the bottom of the raft. However, as the depth increases, the subsoil settlement reduces considerably, while the pile's settlement remains nearly constant. Consequently, beneath the top of the pile, the settlement of the pile always surpasses that of the subsoil, creating positive skin friction across the full length of the piles. Therefore, the peak axial load of the connected pile is located at its top, with a gradual reduction toward the pile's tip.

For the DPR foundation, the mechanism of load transfer is more complex than in the PR foundation, because of the interactions among the raft, piles, subsoil, and cushion. Fig. 1b indicates that the deformation potential of the cushion layer permits relative movement between the raft and the piles (i.e., $w_r > w_p$). At ground level, the settlement of the raft, subsoil and piles is not the same (i.e., $w_r > w_s > w_p$). The subsoil settlement ($w_s$) is greater than the settlement of piles ($w_p$) at the upper depths, therefore negative skin friction mobilizes along the perimeter of the pile. Consequently, the load is transferred to the pile, partly via the negative skin friction generated across the pile's shaft and partly via the pile head. With increasing depth, $w_s$ continues to decrease, while $w_p$ remains nearly constant. At a specific depth below the top of the pile, $w_s$ equals $w_p$, marking the position of the neutral plane. Below this level, $w_s$ becomes less than $w_p$, therefore the load is transmitted from the pile to the adjacent soil through positive skin friction. Therefore, in the DPR system, the pile's axial load first rises with depth, reaching its peak at the neutral plane, then decreases with further depth toward the pile tip.

The current literature highlights that the behavior of DPR system is affected by the complex interactions among the cushion, subsoil, raft, and piles.

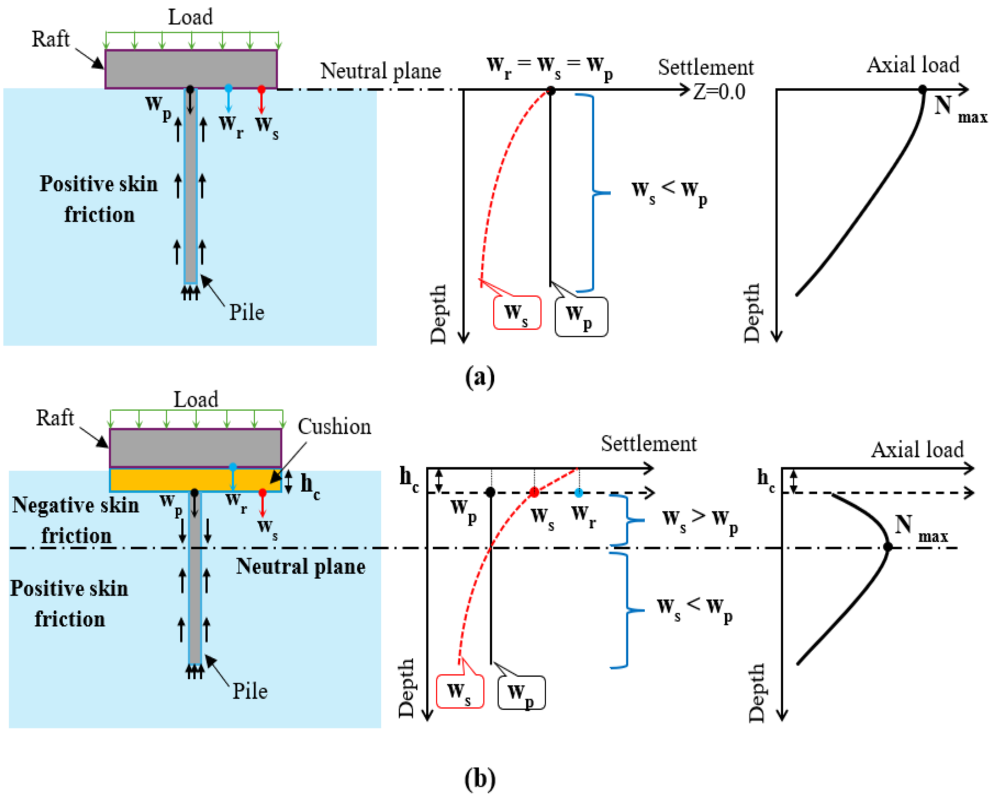


*Fig. 1. Load transfer mechanism: (a) PR, (b) DPR.*

These interactions are still not fully comprehended and require additional research to ensure the development of effective designs and the proper application of DPR in engineering projects.

Therefore, in this research, the performance of the DPR foundation is examined through 3D finite element (FE) model developed with PLAXIS 3D V2020 software [32]. To accurately model the complex interactions, the nonlinear soil behavior is modeled using the Hardening Soil Model and the piles are simulated as volume elements.

First, the FE model's accuracy is verified using the findings of centrifuge tests. Then, the verified model is used in a parametric study to evaluate the influence of some key parameters, including cushion thickness and elasticity modulus, as well as the length and diameter of piles, on the performance of the DPR system resting on loose sand under uniform vertical loads. The load carrying capacity of the DPR foundation, load distribution between the piles and the raft, and axial loads and bending moments induced in the disconnected piles are analyzed and discussed.

## 2. Finite Element Modelling

### 2.1. Numerical Model

This section highlights the main characteristics of the 3D FE model utilized in the parametric analysis to examine the performance of DPR foundation founded on loose sand under uniform vertical loads.

To eliminate the impact of the model boundaries on the foundation performance, the lateral boundaries of the model are extended to twice the raft width, measured from the raft edges. These boundaries are fixed horizontally but are allowed to move vertically. In the vertical direction, the model's bottom boundary is set at a distance twice the length of the pile below the bottom of the raft and is fixed in both horizontal and vertical directions [5]. A schematic cross-section of the geometry for the FE model of the DPR system is presented in Fig. 2.

Owing to the studied foundation's symmetry in both directions, the model represents only one-quarter of the geometry, as illustrated in Fig. 3. This helps reduce the overall model size and, consequently, the computational time required.

To accurately simulate the nonlinear elasto-plastic behavior of loose sand and the granular cushion, they are represented using the Hardening Soil (HS) model. This model incorporates a stress-dependent soil stiffness, which is enhanced by cycles of loading, unloading, and reloading [33]. On the other hand, the raft and concrete piles are represented using the Linear Elastic (LE) model, considering that they stay within an elastic state as a result of their significantly higher stiffness relative to the surrounding soil. In this research, both the raft and the piles are simulated using volume elements to improve the accuracy of the soil-structure interaction simulation. The properties of the soil, cushion, raft, and piles used in the FE analysis are provided in Table (1). The geotechnical properties of the loose sand and the cushion are derived from [34].

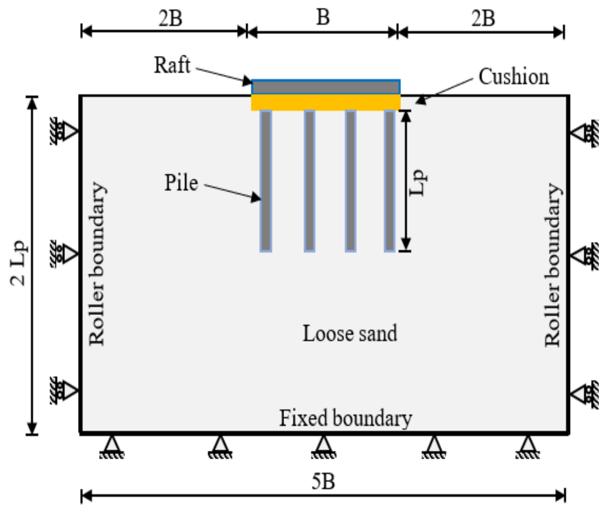


*Fig. 2. A schematic section of the geometry for the FE model of the DPR system.*

To model the interaction among the structural elements and the adjacent soil, interface elements are used to capture their relative movement. These interface elements are considered to have zero thickness, and their shear strength characterized by the interface reduction factor ($R_{inter}$). This factor expresses the interface strength as a proportion of the surrounding soil's shear strength. In the present research, $R_{inter}$ is taken as 0.67 for sandy soil, as proposed by [35].

To improve the accuracy of the results, a very fine meshing scheme is chosen for the entire model. Moreover, local refinement is implemented near the structure elements where significant stress or deformation is expected.

The DPR system construction process is simulated by dividing the numerical calculations into three distinct stages. In the initial stage, the geostatic stresses are computed through the K0-procedure as the soil volume is activated. The second stage involves the construction of the piles, cushion, raft, and interfaces. In the final stage, the load is imposed on the raft's top surface.

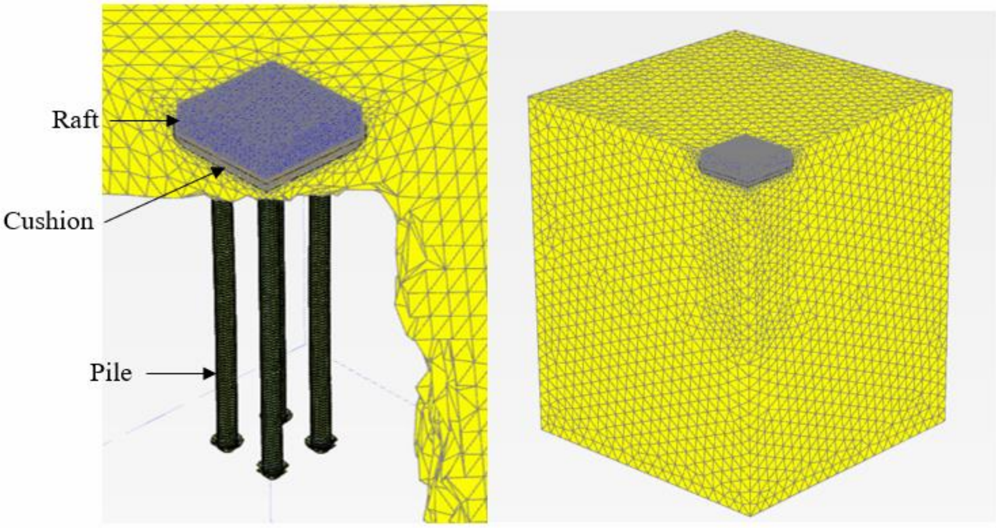


*Fig. 3. One- quarter of the 3D FE model of DPR system.*

*Table 1. Material properties used in the FE analysis.*

| Material | Soil (loose sand) | Cushion | Raft & piles | Units |
|---|---|---|---|---|
| **Model** | **HS** | **HS** | **LE** | **-** |
| **Drainage type** | **Drained** | **Drained** | **Non-porous** | **-** |
| $D_r$ | 30 | 80 | - | % |
| $\gamma_{sat}, \gamma_{unsat}$ | 16.0 | 18.0 | 25.0 | $kN/m^3$ |
| $\nu$ | 0.2 | 0.2 | 0.15 | - |
| $E$ | - | - | 22.0 e6 | $kN/m^2$ |
| $E_{oed}$ | 18000 | 48000 | - | $kN/m^2$ |
| $E_{50}$ | 18000 | 48000 | - | $kN/m^2$ |
| $E_{ur}$ | 54000 | 144000 | - | $kN/m^2$ |
| $m$ | 0.60 | 0.50 | - | - |
| $c$ | 0.1 | 0.1 | - | $kN/m^2$ |
| $\varphi$ | 30 | 38 | - | Degrees |
| $\psi$ | 0 | 8 | - | Degrees |
| $R_f$ | 0.96 | 0.90 | - | - |
| $R_{inter}$ | 0.67 | 0.67 | - | - |

### 2.2. MODEL VALIDATION

The results of the centrifuge tests in sandy soil conducted by [24] are employed to verify the present 3D FE model. These centrifuge experiments were conducted on three different foundation systems, including the unpiled raft, PR foundation, and DPR foundation, at 50 g of centrifugal acceleration.

In the prototype scale, for each test model, a 7.5 m square rigid raft with a thickness of 2.0 m is used. For the DPR and PR systems, the raft is carried by nine piles with a 1.0 m diameter and 20 m length. These piles are arranged in a 3 × 3 square pattern, with uniform spacing of 2.5 m. In the DPR system, a gravel cushion with a thickness of 1.0 meter is placed beneath the raft. To achieve a settlement of 20 cm, concentrated vertical loads of 22 MN, 63 MN, and 73 MN are applied on the raft's central for the unpiled raft (UR), DPR, and PR systems, respectively. The soil beneath the raft is sand of 50% relative density.

In the scaled models, aluminum piles are utilized to mimic the performance of prestressed high-strength concrete (PHC) piles. The pile characteristics for the model and prototype scales are provided in Table (2).

PLAXIS 3D is used to perform the FE analysis, maintaining the same material properties, geometry, and dimensions as those in the centrifuge tests. Table 3 presents the material characteristics applied in the FE analysis.

The comparison of load-settlement curves obtained from the current FE analyses with those from the centrifuge tests for UR, DPR, and PR is presented in Fig. 4. The results from the FE analysis demonstrate good consistency with the centrifuge test results. This validation supports the capability of the employed numerical model to examine the behavior of the DPR foundation on sandy soil.

*Table 2. Properties of pile model [24].*

| Testing model | Pile | |
|---|---|---|
| | **Prototype** | **Model at 50 g** |
| **Material** | PHC | Aluminum |
| **Diameter** | 1 m | 20 mm |
| **Thickness** | - | 2 mm |
| **Length** | 20 | 400 mm |
| **Axial rigidity** | $2.16 \times 10^{10}$ N | $7.98 \times 10^{6}$ N |
| **Flexural rigidity** | $1.35 \times 10^{9}$ N. m$^2$ | $3.27 \times 10^{2}$ N. m$^2$ |

*Table 3. Material properties used in the model validation.*

| Parameter | Sand | Gravel cushion | Raft and piles | Units |
|---|---|---|---|---|
| Material Model | HS | HS | LE | - |
| Drainage type | Drained | Drained | Non-porous | - |
| $\gamma_{sat}$, $\gamma_{unsat}$ | 14.0 | 20.0 | 26.5 | $kN/m^3$ |
| $\nu$ | 0.2 | 0.2 | 0.2 | - |
| $E$ | - | - | 27.5 e6 | $kN/m^2$ |
| $E_{oed}$ | 20000 | 80000 | - | $kN/m^2$ |
| $E_{50}$ | 20000 | 80000 | - | $kN/m^2$ |
| $E_{ur}$ | 80000 | 240000 | - | $kN/m^2$ |
| $m$ | 0.65 | 0.50 | - | - |
| $c$ | 0.1 | 0.1 | - | $kN/m^2$ |
| $\varphi$ | 34 | 38 | - | Degrees |
| $\psi$ | 4 | 8 | - | Degrees |
| $R_{inter}$ | 0.67 | 0.67 | - | - |

### 2.3. PARAMETRIC STUDY

3D FE analyses are performed to examine the behavior of DPR system founded on loose sand under uniform vertical loading. In the studied DPR foundation, a small number of disconnected floating piles are installed below the raft to reduce settlement within permissible limits. These disconnected floating piles primarily serve as settlement-reducing elements. The principal aim of the current parametric study is to investigate the impact of various parameters, incorporating cushion thickness, cushion modulus of elasticity, pile length, and pile diameter, on the behavior of the DPR foundation.

The DPR model used in the parametric study is presented in Fig. 5. It consists of a square rigid raft with dimensions of 11.5 m × 11.5 m × 1.5 m, supported by 16 disconnected floating piles distributed uniformly in a 4 × 4 grid arrangement, with constant spacing of 3.0 m. While the pile length ($L_p$), pile diameter ($d_p$), cushion thickness ($h_c$), and the elastic modulus of the cushion ($E_c$) are changed through the analyses. A uniform vertical load of 200 kPa is applied to the raft, which represents the working load typically associated with multi-story buildings. The middle Pile is denoted by the abbreviation MP, as shown in Fig. 5.

Table 4 provides a summary of the DPR models used in the parametric study and the analyzed parameters. During the parametric study, just a single parameter is varied individually, while the remaining parameters are held constant at their reference values.

## 3. RESULTS AND DISCUSSION

In this section, the findings from the parametric study are introduced and discussed, addressing the load–settlement performance of the DPR foundation, the load distribution among the piles and the raft, and the piles' axial load and bending moment.

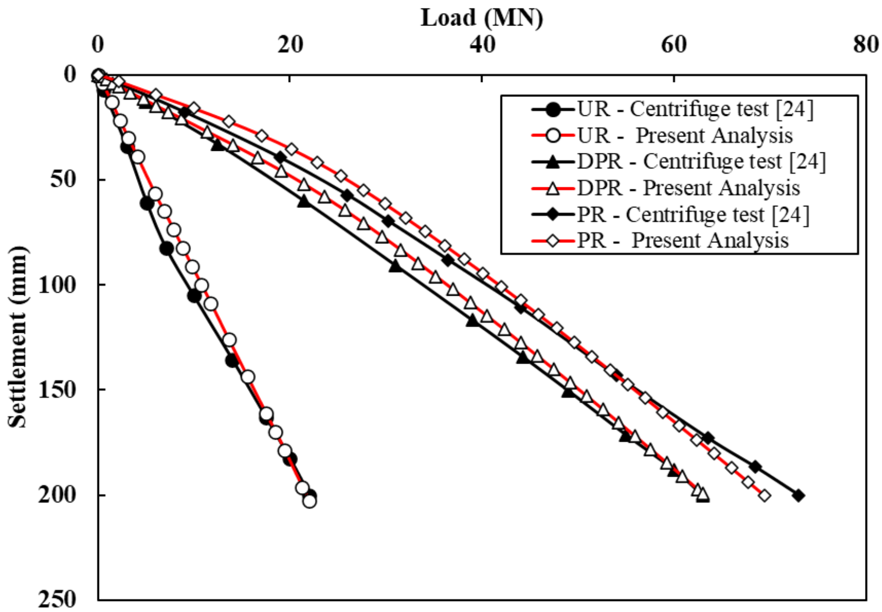


*Fig. 4. Comparison of load settlement behavior of the present study with the reported results [24].*

*Table 4. Summary of studied DPR models in the parametric study.*

| Parametric study | Raft | Cushion | | Floating pile group | | | |
|---|---|---|---|---|---|---|---|
| | $B_r \times L_r \times t_r$ (m) | $h_c$ (m) | $E_c$ (MPa) | $n_p$ | $S$ (m) | $d_p$ (m) | $L_p$ (m) |
| **Cushion thickness** | 11.5×11.5× 1.5 | 0.0<br>0.25<br>0.50<br>0.75<br>1.00<br>1.25<br>1.50<br>1.75 | 48 | 4×4 | 3.0 | 0.5 | 17.5 |
| **Cushion modulus of elasticity** | 11.5×11.5× 1.5 | 0.5 | 18<br>30<br>48<br>120<br>22000 | 4×4 | 3.0 | 0.5 | 17.5 |
| **Pile length** | 11.5×11.5× 1.5 | 0.5 | 48 | 4×4 | 3.0 | 0.5 | 5.75 (0.5 $B_r$)<br>8.625 (0.75 $B_r$)<br>11.50 ($B_r$)<br>17.50 (1.52 $B_r$)<br>23.00 (2.0 $B_r$)<br>28.75 (2.5 $B_r$) |
| **Pile diameter** | 11.5×11.5× 1.5 | 0.5 | 48 | 4×4 | 3.0 | 0.3<br>0.4<br>0.5<br>0.6 | 17.5 |

$B_r$: raft width, $L_r$: raft length, $t_r$: raft thickness,
$h_c$: cushion thickness, $E_c$: cushion modulus of elasiticty, $n_p$: number of piles,
$S$: pile spacing, $d_p$: pile diameter, $L_p$: pile length,

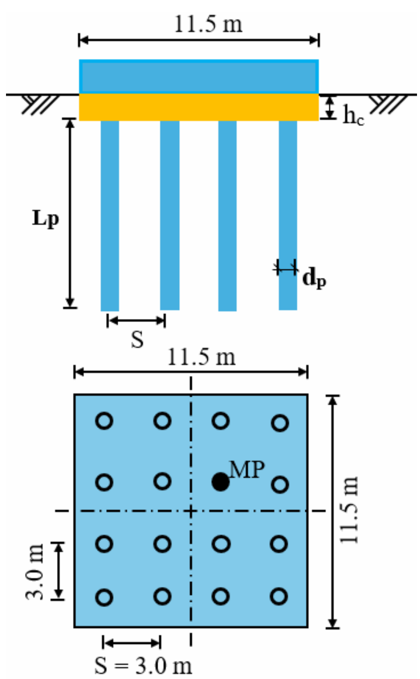


*Fig. 5. Schematic diagram of the DPR model used in the parametric study.*

### 3.1. INFLUENCE OF CUSHION THICKNESS ON DPR FOUNDATION

Numerical simulations are conducted for a square rigid raft with dimensions of 11.5 m × 11.5 m × 1.5 m supported on 16 disconnected floating piles with pile spacing of 6 $d_p$. Each pile has a diameter ($d_p$) of 0.5 m, and its length ($L_p$) is 17.5 m. The cushion layer has an elastic modulus ($E_c$) of 48 MPa. The cushion thickness ($h_c$) is varied from 0.25 to 1.75 m.

#### 3.1.1. LOAD-SETTLEMENT BEHAVIOR

Fig. 6 depicts the load–settlement curves of the unpiled raft (UR), PR (corresponding to $h_c$= 0), and DPR with different cushion thicknesses under a uniform vertical load of 200 kPa. For all the studied cases, the settlement was measured at the raft's center. It is observed that under the maximum applied load, the raft's settlement is significantly reduced to an allowable value for all the studied PR and DPR foundations.

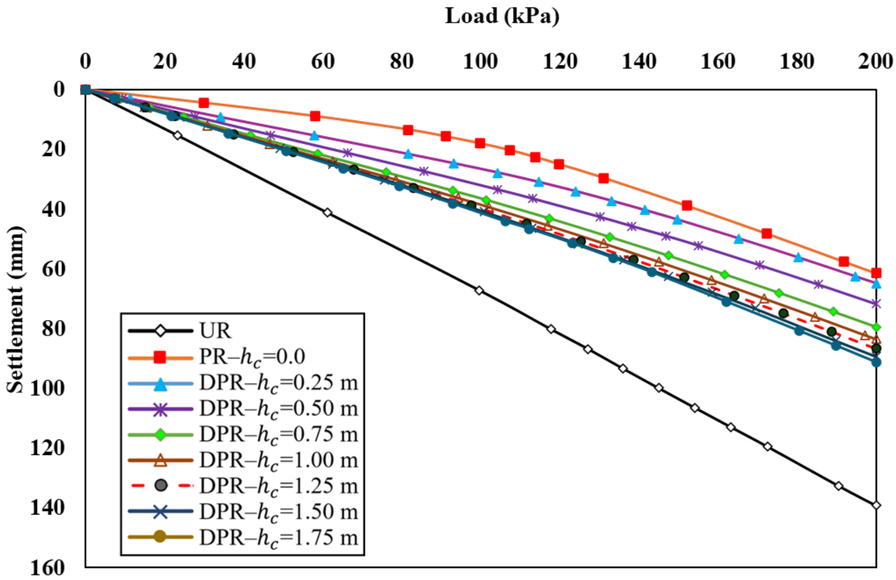


*Fig. 6. Load–settlement curves for UR and DPR with different cushion thickness.*

However, the maximum settlements of the different DPR are higher than those of the PR. Furthermore, it is evident that the settlement of the DPR system increases as $h_c$ increases. This occurs because the increase in cushion thickness results in less load being transmitted to the piles and more load to the topsoil, thereby increasing the settlement of the DPR foundation. These results align with the findings reported in [30].

The effectiveness of PR and DPR systems in minimizing raft settlement can be assessed through a dimensionless parameter known as the settlement efficiency ($\eta$) [25], as defined by $Eq.$ 1. In this context, $w_r{}^{up}$ represents the settlement of the raft without piles, while $w_r$ refers to the settlement with piles, whether connected or disconnected, under the same applied load.

$$\eta = \frac{w_r{}^{up} - w_r}{w_r{}^{up}} \quad (1)$$

The ($\eta$) at the maximum load is graphed versus the thickness of the cushion in Fig. 7. It is evident that settlement efficiency decreases as the $h_c$ increases. Increasing the $h_c$ from 0.0 to 0.75 m leads to 12.9 % reduction in the (η). Further increases in $h_c$, from 0.75 m to 1.75 m, result in a slower rate of decline, with the ($\eta$) decreasing by only 8.5%. This indicates that $h_c$ beyond 0.75 m has a diminishing impact on settlement efficiency, and its effectiveness appears to be minimal.

### 3.1.2. LOAD SHARING BEHAVIOR

In both DPR and PR systems, the applied load is distributed among the piles and the raft. The proportion of the load shared by the raft and the piles is typically presented as ratios of the overall imposed load on the foundation system. According to the findings from the FE simulations, the load supported by the piles is computed by dividing the total load of the pile tops by the overall applied load. Then, to determine the load transmitted to the raft, the load supported by the piles is subtracted from 1.

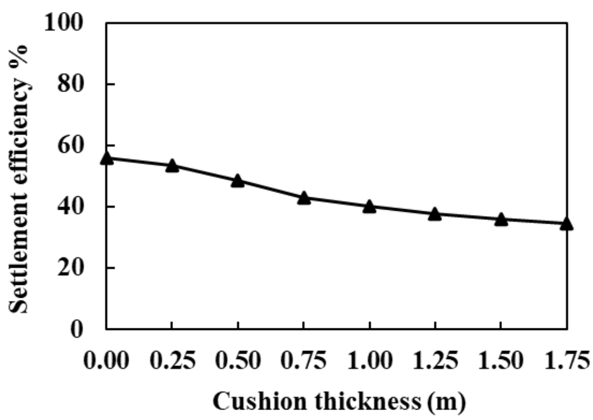


*Fig. 7. Influence of cushion thickness on the settlement efficiency of DPR at a load of 200 kPa.*

Fig. 8 depicts the variation in the load distribution among the raft and the piles with the $h_c$ at a load of 200 kPa. It is noted that the load supported by the piles reduces, whereas the load carried by the raft increases as the $h_c$ increases. This is because the increased cushion thickness reduces stress concentration at the pile heads, resulting in a more uniform stress distribution and thereby a reduction in the load supported by the piles, this behavior matches the results described in [31].

It is noted that in the case of the PR system, the piles carry 67.4% of the total applied load, while the raft shares 32.6%. In contrast, for the DPR foundation, the load supported by the piles reduces sharply from 67.4% to 37.1% as the $h_c$ increases from 0.0 to 0.5 m. This decrease then becomes more gradual, with the load shared by the piles reducing from 37.1% to 26.3% as $h_c$ increases from 0.5 to 1.0 m. For the $h_c$ values greater than 1.0 m, a minor reduction in the load transferred to the piles ($P\%$) is observed. This implies that increasing cushion thickness beyond 1.0 m has a limited influence on the load sharing mechanism within the studied DPR foundation.

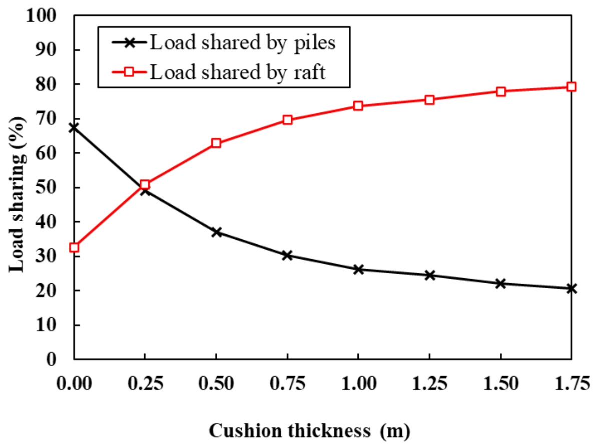


*Fig. 8. Influence of cushion thickness on the load sharing of DPR at a load of 200 kPa.*

### 3.1.3. Axial Load Distribution Along the Pile

Fig. 9 illustrates the influence of $h_c$ on the axial load distribution through the depth of the middle pile within the DPR foundation. It is noted that for the PR case (i.e., $h_c$= 0), the highest axial load in the pile is located at its top and subsequently gradually reduces as the depth of the pile increases. This pattern is a result of the positive skin friction generated along the entire pile shaft; this distribution aligns with the observation in Fig. 1a. On the other hand, for the DPR system with any value of $h_c$, the peak axial load on the pile is not located at the top but at some depth beneath the top of the pile, where the neutral plane is situated. This occurs because negative skin friction is mobilized across the pile above the neutral plane; this behaviour is similar to that observed in Fig. 1b.

Additionally, it is observed that as the $h_c$ increases, both the pile load at its head ($N_{head}$) and the maximum pile load at the neutral plane ($N_{max}$) decrease; a similar observation is reported in [22] Moreover, the axial load at the pile tip remains constant at 253 kN, regardless of the cushion thickness.

Fig. 9 further indicates that the neutral plane is situated at the pile top for the PR system, while for the DPR foundation, the neutral plane shifts downward as the $h_c$ increases. The depth of the neutral plane, measured from the ground surface ($Z_{np}$), can be normalized by the pile length ($L_p$) to obtain the depth ratio of the neutral plane, $Z_{np}/L_p$. Fig. 10 shows the influence of $h_c$ on the $Z_{np}/L_p$ ratio. It is clear that as $h_c$ increases from 0.0 m to 0.75 m, the neutral plane moves downward to a position at 43% of the pile length. After $h_c$ exceeds 0.75 m, the further downward movement of the neutral plane becomes limited.

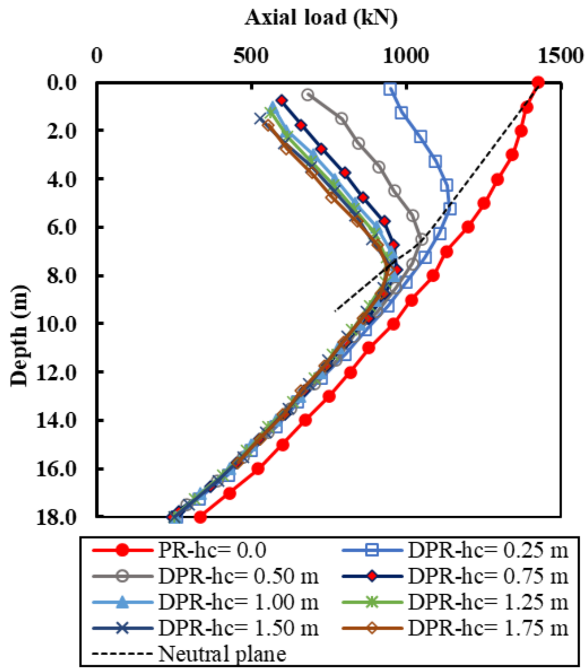


*Fig. 9. Influence of cushion thickness on axial load distribution along the middle pile.*

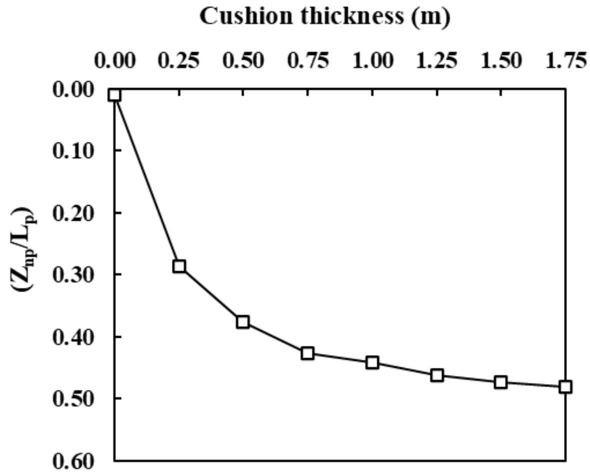


*Fig. 10. Influence of cushion thickness on the depth of the neutral plane for the middle pile.*

The reduction in axial load through the pile, both at the pile head and at the neutral plane, as the cushion thickness increases, could be quantified using two dimensionless parameters. The first parameter ($NR_{head}$ ) referred to as the normal force ratio at the pile head, is the ratio of the axial load at the pile head in case of DPR foundation to that in PR system. The second parameter ($NR_{np}$), called the maximum normal force ratio, represents the ratio of the maximum axial load in case of DPR system to that in PR system. The influence of $h_c$ on the two normal force ratios, $NR_{head}$ and $NR_{np}$ for the middle pile is presented in Fig. 11. It is apparent that, as $h_c$ increases from 0 to 0.5 m, there is a significant decrease in both the axial load at the pile head and the maximum axial load on the pile (with a 52% reduction at the pile head and a 28% drop in the maximum axial load). However, when the $h_c$ exceeds 0.5 m, the reduction in both normal force ratios becomes minimal.

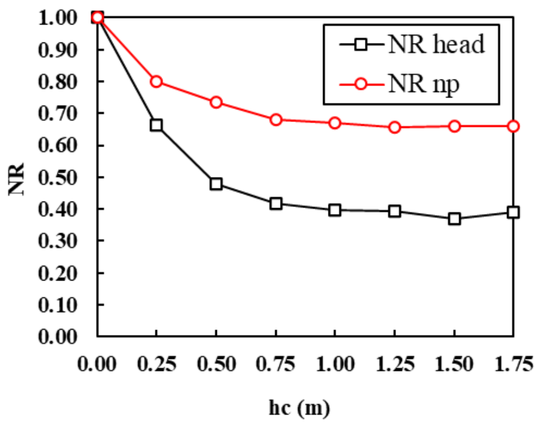


*Fig. 11. Influence of cushion thickness on normal force ratios for the middle pile.*

### 3.1.4. BENDING MOMENT DISTRIBUTION ALONG THE PILE

Fig. 12 demonstrates the impact of $h_c$ on the bending moment distribution across the middle pile in the DPR system. For the case of $h_c$ = 0.0 (PR system), the highest bending moment takes place at the pile top because the piles and the raft are rigidly connected, while the moment decreases to nearly zero at the pile tip. However, for the DPR foundation, regardless of the value of $h_c$, the bending moment is almost zero at both pile ends, and the highest bending moment occurs at some depth beneath the top of the pile, with a lower value compared to that in the PR foundation; this moment distribution is consistent with that reported by [20].

The decrease in bending moment across the pile length as the $h_c$ increases could be captured by two dimensionless parameters. The first parameter, ($MR_{head}$), referred to as the bending moment ratio at the pile head, is the ratio of the bending moment at the pile head in case of DPR foundation to that in PR system. The second parameter, ($MR_{max}$), called the maximum bending moment ratio, compares the highest bending moment in the DPR to that in the PR.

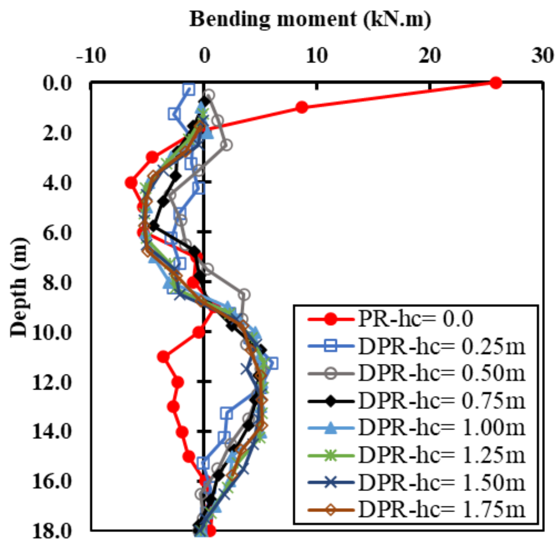


*Fig. 12. Influence of cushion thickness on bending moment distribution along the middle pile.*

Fig. 13 presents the impact of $h_c$ on the two bending moment ratios, $MR_{head}$ and $MR_{max}$, for the middle pile in the DPR system. The bending moment at the pile top reduces by 95% as the $h_c$ rises from 0.0 m (PR case) to 0.25 m. When the $h_c$ further increases to 0.5 m, the bending moment at the pile top becomes nearly zero and remains constant at this values for all higher cushion thicknesses. However, the maximum bending moment reduces by 73% as the $h_c$ rises from 0.0 m (PR case) to 0.25 m. Once the cushion thickness reaches 0.5 m, the maximum bending moment stabilizes with a reduction of 80% relative to the PR system.

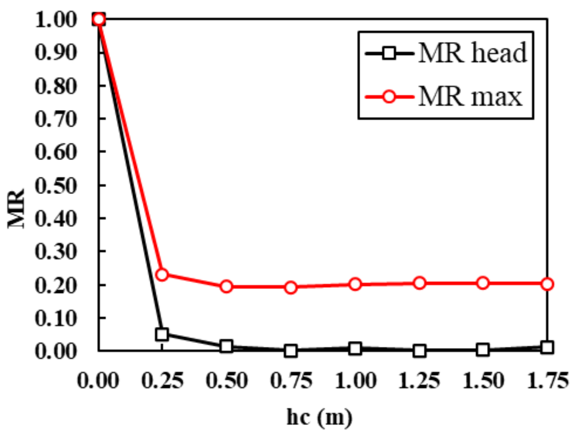


*Fig. 13. Influence of cushion thickness on bending moment ratios (MR) for the middle pile.*

The findings indicate that increasing the cushion thickness causes a decrease in both the axial load and bending moments generated in the piles (as illustrated in Figs. 9, 12). However, this increase in thickness also results in a higher settlement of the DPR system (as shown in Figs. 6, 7). Consequently, selecting the appropriate cushion thickness for a cost-effective DPR system should involve careful engineering assessment, aiming for an ideal balance between these factors.

According to the results of this section, it is recommended that, for optimal performance of the DPR system, the cushion thickness should be between 0.5 m and 1.0 m. In the following sections, a cushion thickness of 0.50 m is selected.

### 3.2. Influence of Cushion Elastic Modulus on DPR Foundation

Numerical analyses are performed for a square rigid raft of 11.5 m × 11.5 m × 1.5 m, supported by 16 disconnected floating piles. The piles are arranged with a spacing of 6 times their diameter, with each pile having a diameter ($d_p$) of 0.5 m and a length ($L_p$) of 17.5 m. The cushion layer has a thickness ($h_c$) of 0.5 m. The influence of the cushion elastic modulus on the performance of the DPR is examined by changing the Young's modulus of the cushion ($E_c$) within a range from 18 MPa (representing the subsoil material) to 22,000 MPa (representing concrete material).

#### 3.2.1. Load-Settlement Behavior

Fig. 14 shows the load–settlement curves of the unpiled raft (UR), PR, and DPR with different values of the cushion elastic modulus ($E_c$) under the same uniformly distributed vertical load of 200 kPa. It is clear that under the maximum applied load, the settlement of the raft is considerably reduced to a tolerable level for all the PR and DPR foundations considered. Additionally, the maximum settlement of the DPR system decreases as $E_c$ increases. This indicates that higher values of the cushion elastic modulus result in a greater load transmitted to the piles and a lower load transmitted to the topsoil, thereby minimizing the settlement of the DPR foundation; this behavior matches the finding reported in [18]. Furthermore, the load–settlement curve of DPR with $E_c$ of 22,000 MPa coincides with that of the PR system.

Fig. 15 illustrates the impact of $E_c$ on settlement efficiency ($\eta$) at the maximum applied load. It is evident that the $\eta$ rises with the increase of cushion elastic modulus. Increasing $E_c$ from 18 MPa (representing loose sand) to 48 MPa (typical of dense sand) leads to an increase in settlement efficiency ($\eta$) by 18.9 %. However, further increases in cushion elastic modulus, from 48 MPa (dense sand) to 22,000 MPa (similar to concrete), result in a significantly slower rate of improvement, with only a 7.3 % increase in settlement efficiency. This suggests beyond 48 MPa, further increases in the cushion elastic modulus have a diminishing impact on settlement efficiency, and its effectiveness appears to be minimal. Therefore, dense sand is recommended as a more suitable and cost-effective material for managing settlements of the studied DPR foundation.

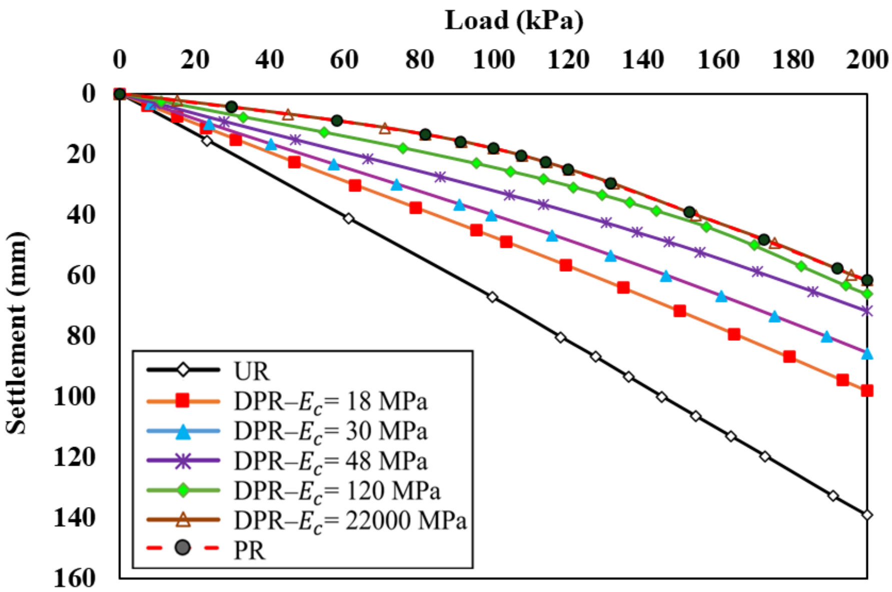


*Fig. 14. Load–settlement curves of the UR, PR, and DPR with different values of the cushion elastic modulus.*

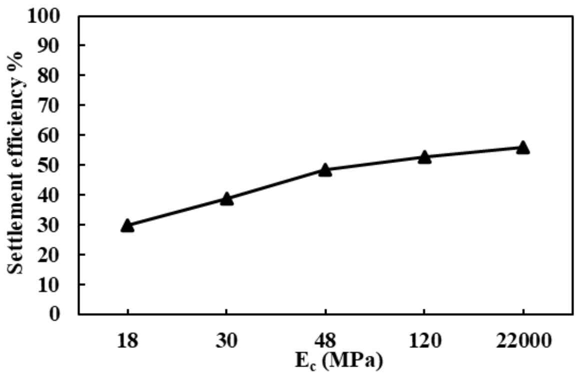


*Fig. 15. Influence of cushion elastic modulus ($E_c$ ) on the settlement efficiency of DPR at a load of 200 kPa.*

### 3.2.2. LOAD SHARING BEHAVIOR

Fig. 16 shows the variation in the load distribution among the raft and the piles with respect to the cushion elastic modulus at load level 200 kPa. The results indicate that as $E_c$ increases, the load transmitted to the piles rises, whereas the load transferred to the raft reduces. It is observed that, when a soil cushion with a low elastic modulus is used, the raft supports the main part of the total load. For example, for a cushion with $E_c$ of 18 MPa, the piles carry only 19.6% of the total applied load, while the raft shares 80.6%. In contrast, when using a concrete cushion with a high elastic modulus, the piles support a higher proportion of the load, (i.e., for cushion with $E_c$ of 22,000 MPa, piles carry 64.6% of the total load, while the raft shares 35.4%).

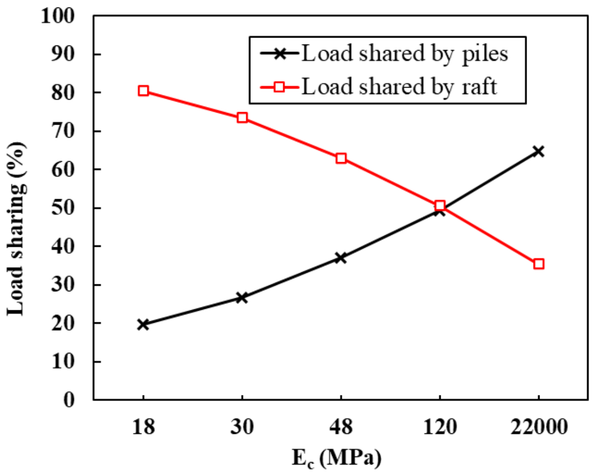


*Fig. 16. Influence of cushion elastic modulus ($E_c$ ) on the load sharing of DPR at a load of 200 kPa.*

### 3.2.3. AXIAL LOAD DISTRIBUTION ALONG THE PILE

Fig. 17 illustrates the influence of $E_c$ on the axial load distribution across the depth of the middle pile in the DPR foundation. For the case of DPR, when using a concrete cushion with an elastic modulus of 22,000 MPa, the axial load distribution across the depth of the disconnected pile is consistent with that of the connected pile in the PR system, i.e., the maximum axial load takes place at the pile top and then gradually decreases towards the pile tip.

In contrast, for cases in which the $E_c$ values represent soil conditions, the position of the highest axial load is moved downward to the position of the neutral plane. Additionally, it is observed that both the axial load at the pile head ($N_{head}$) and the maximum axial load at the neutral plane ($N_{max}$) increase as $E_c$ increases. Moreover, the axial load at the pile tip remains almost constant at 260 kN, regardless of the cushion elastic modulus, meaning that the elastic modulus of the cushion has minimal impact on axial load at the pile tip.

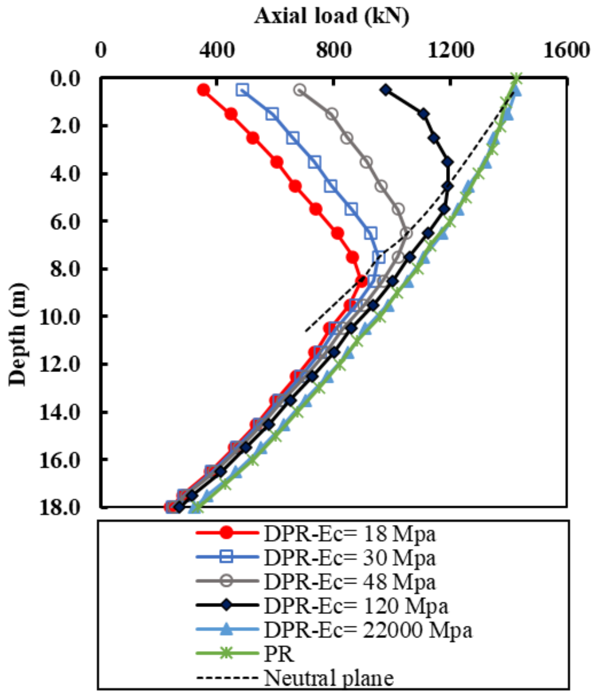


*Fig. 17. Influence of cushion elastic modulus ($E_c$ ) on axial load distribution along the middle pile.*

The influence of $E_c$ on the depth ratio of the neutral plane ($Z_{np}/L_p$) is presented in Fig. 18. It is observed that for the DPR system with a concrete cushion having an $E_c$ of 22,000 MPa, the neutral plane is positioned at the pile head, directly beneath the cushion. In contrast, for lower values of $E_c$, the neutral plane tends to move downwards (e.g., the $Z_{np}/L_p$ ratios are 0.24, 0.38, and 0.49 for $E_c$ values of 120, 48, and 18 MPa, respectively).

The impact of $E_c$ on the two normal force ratios, $NR_{head}$ and $NR_{np}$ for the middle pile is depicted in Fig. 19. It is evident that for the DPR system with a concrete cushion having an $E_c$ of 22,000 MPa, there is no reduction in the axial force at the pile top with respect to the PR foundation. This suggests that concrete is ineffective as a cushion material, as it does not contribute to optimizing the stress distribution between the piles and subsoil. On the other hand, for lower values of $E_c$, within the range of typical soil materials, there is a significant decrease in both the axial force at the pile top and the peak axial force on the pile as $E_c$ decreases (e.g., as $E_c$ reduces from 22,000 MPa to 18 MPa, $NR_{head}$ drops from 1 to 0.25, and $NR_{np}$ reduces from 1 to 0.63).

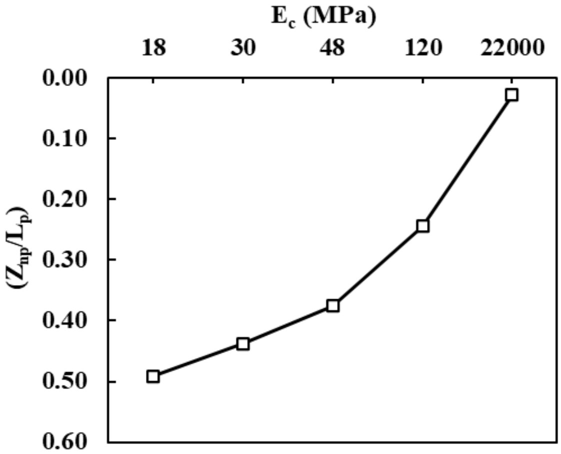


*Fig. 18. Influence of cushion elastic modulus ($E_c$ ) on the depth of the neutral plane for the middle pile.*

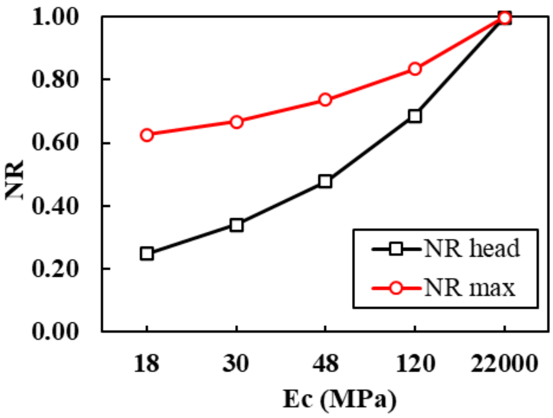


*Fig. 19. Influence of cushion elastic modulus ($E_c$ ) on normal force ratios for the middle pile.*

### 3.2.4. Bending Moment Distribution Along the Pile

Fig. 20 illustrates the influence of the $E_c$ on the bending moment distribution across the depth of the middle pile in the DPR foundation. It is evident that when the DPR system includes a concrete cushion with an $E_c$ of 22,000 MPa, the bending moment profile across the depth of the disconnected pile closely resembles that of the connected pile in the PR system. In both cases, the highest bending moment occurs at the pile top, with only slight differences in magnitude between the two systems, while the moment approaches zero at the pile tip. Conversely, for lower values of $E_c$, which are typical for soil materials, the bending moment is nearly zero at both ends of the pile, with the peak bending moment occurring at a depth beneath the pile top, and its magnitude is lower compared to that in the PR foundation.

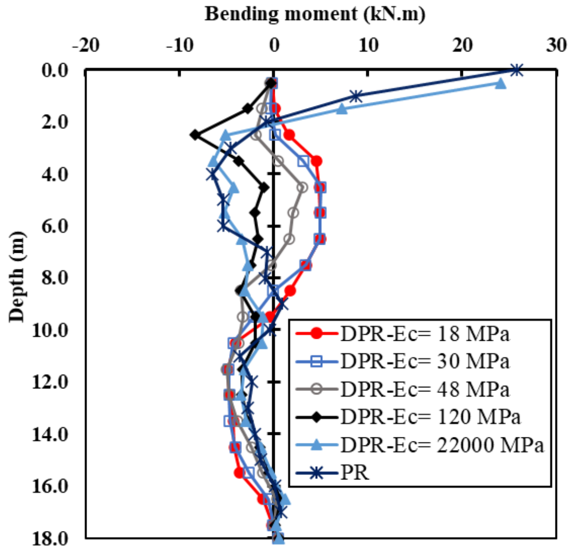


*Fig. 20. Influence of cushion elastic modulus ($E_c$ ) on bending moment distribution along the middle pile.*

Fig. 21 shows the variation in the bending moment ratios ($MR$) versus the cushion elastic modulus ($E_c$). It is noticed that $MR_{head}$ experiences a sharp decrease from 0.93 to 0.01 as $E_c$ reduces from 22,000 MPa to 120 MPa, after which it remains almost constant at 0.01 for lower values of $E_c$. On the other hand, $MR_{max}$ shows a rapid decrease from 0.93 to 0.32 as $E_c$ reduces from 22,000 MPa to 120 MPa, followed by a slower reduction from 0.32 to 0.20 as $E_c$ decreases further from 120 MPa to 48 MPa, and finally, it stabilizes at 0.19 for the lower values of $E_c$.

According to the findings in this section, a cushion with an elastic modulus of 48 MPa is suggested to achieve the best performance in the studied DPR system.

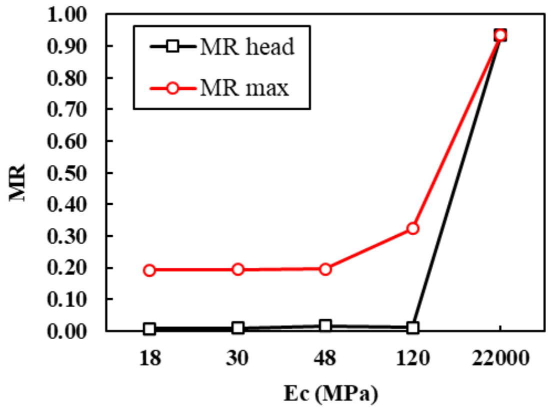


*Fig. 21. Influence of cushion elastic modulus ($E_c$ ) on bending moment ratios ($MR$) for the middle pile.*

### 3.3. INFLUENCE OF PILE LENGTH ON DPR FOUNDATION

Numerical simulations are performed for a square rigid raft of 11.5 m × 11.5 m × 1.5 m supported on 16 disconnected floating piles with pile spacing of 6 $d_p$. All piles have a diameter ($d_p$) of 0.5 m. The cushion layer has a thickness ($h_c$) of 0.5 m and a Young's modulus ($E_c$) of 48 MPa. The effect of the length of the pile, represented as a percentage of the width of the raft, $L_p/B_r$, on the behavior of the DPR is investigated by varying the $L_p/B_r$ ratio from 0.5 to 2.5.

#### 3.3.1. LOAD-SETTLEMENT BEHAVIOR

Fig. 22 illustrates the load–settlement curves of the DPR for various values of $L_p/B_r$ ratio. For comparison purposes, the load–settlement curve of the unpiled raft is provided as well. The findings indicate that as the $L_p/B_r$ ratio rises, the settlement of the DPR system decreases. This is attributed to the increase in pile length, which leads to a greater contact surface area with the surrounding soil, resulting in enhanced skin friction, which, in turn, improves the load-bearing capacity of both the pile and the DPR system; this behavior is similar with the findings reported in [18]. However, it is noteworthy that the highest settlement exceeds the allowable limits for $L_p/B_r$ ratios of 0.5, 0.75, and 1.

The impact of the $L_p/B_r$ ratio on settlement efficiency ($\eta$) at the maximum applied load is shown in Fig. 23. It is apparent that increasing the $L_p/B_r$ ratio improves the settlement efficiency. Increasing the $L_p/B_r$ ratio from 0.5 to 1 causes a 16.5% increase in $\eta$, but the settlement remains above the allowable limits. A more significant improvement is observed when the ratio is increased from 1 to 2, yielding a 32.6% increase in $\eta$. However, further increases in the ratio, from 2 to 2.5, lead to a smaller gain in settlement efficiency, with only 3%.

#### 3.3.2. LOAD SHARING BEHAVIOR

Fig. 24 illustrates how the $L_p/B_r$ ratio affects the load distribution among the raft and the piles at a load of 200 kPa for DPR system. The findings indicate that as the $L_p/B_r$ ratio rises, the piles' load grows, and the load transferred to the raft reduces. This suggests that as the pile length increases, the pile experiences less settlement as it generates more skin friction, leading to a greater load being borne by the pile. But the impact of pile length on the load supported by the piles becomes less significant as the $L_p/B_r$ ratio exceeds 1.5. For instance, the piles' load rose by nearly 19% as the $L_p/B_r$ ratio increased from 0.5 to 1.5, while it increased by only about 7.6 % as the $L_p/B_r$ ratio increased from 1.5 to 2.5.

#### 3.3.3. AXIAL LOAD DISTRIBUTION ALONG THE PILE

Fig. 25 demonstrates the effect of the $L_p/B_r$ ratio on the axial load distribution across the depth of the middle pile in the DPR foundation. The results show that as the $L_p/B_r$ ratio increases, both the axial load at the pile head ($N_{head}$) and the maximum axial pile load at the neutral plane ($N_{max}$) also increase. Additionally, it is observed that the neutral plane moves downward with increasing the $L_p/B_r$ ratio.

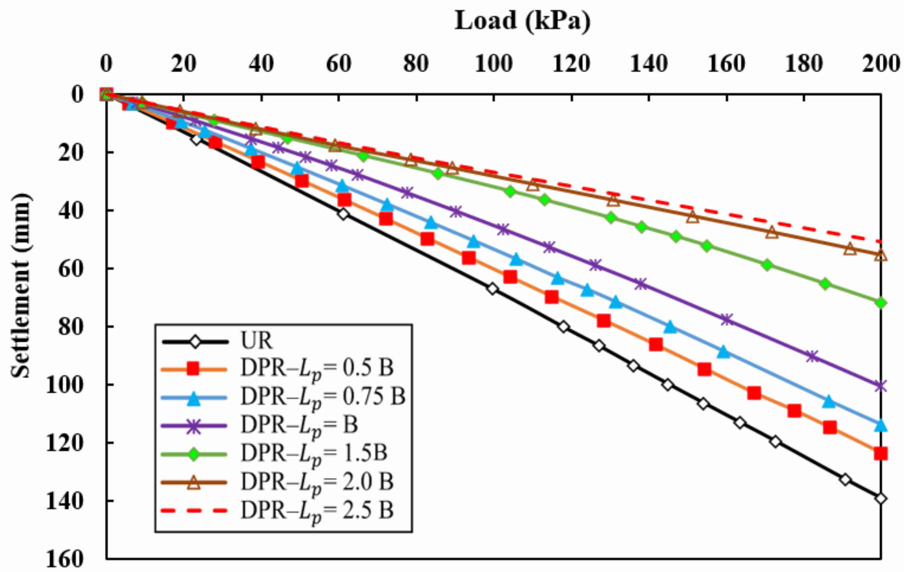


*Fig. 22. Load–settlement curves of the UR, and DPR with different pile lengths.*

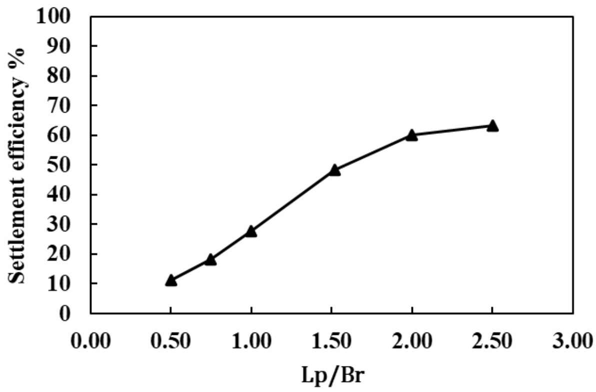


*Fig. 23. Influence of pile length on settlement efficiency of DPR at a load of 200 kPa.*

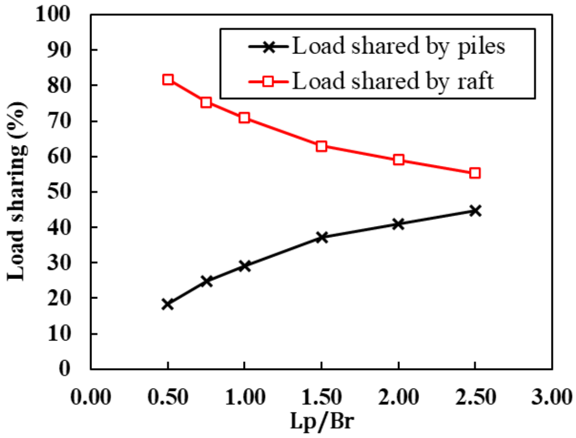


*Fig. 24. Influence of pile length on the load sharing of DPR at a load of 200 kPa.*

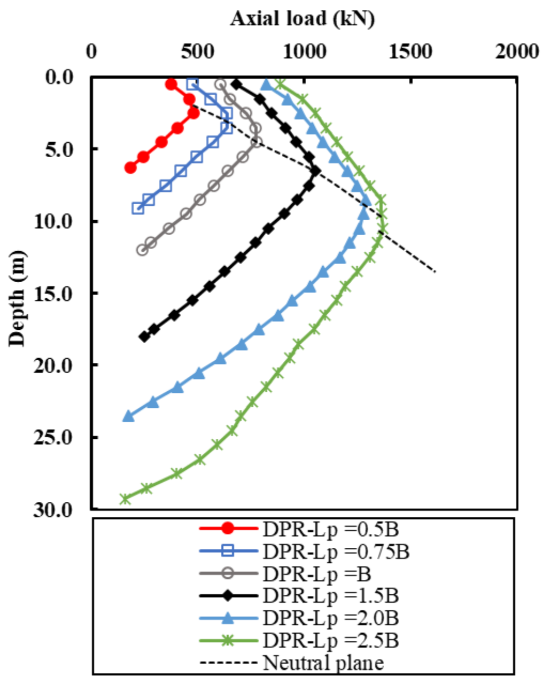


*Fig. 25. Influence of pile length on axial load distribution along the middle pile.*

As shown in Fig. 26, $N_{head}$ increases by 61%, 12.5%, 20.2%, and 8.4% as the $L_p/B_r$ ratio increases from 0.5 to 1, from 1 to 1.5, from 1.5 to 2, from 2 to 2.5, respectively. Meanwhile, $N_{max}$ increased by 61.9 %, 35.7%, 22.8%, and 6.2% over the same intervals of the $L_p/B_r$ ratio. It is evident that the impact of pile length on both $N_{head}$ and $N_{max}$ becomes less significant as the $L_p/B_r$ ratio exceeds 2.

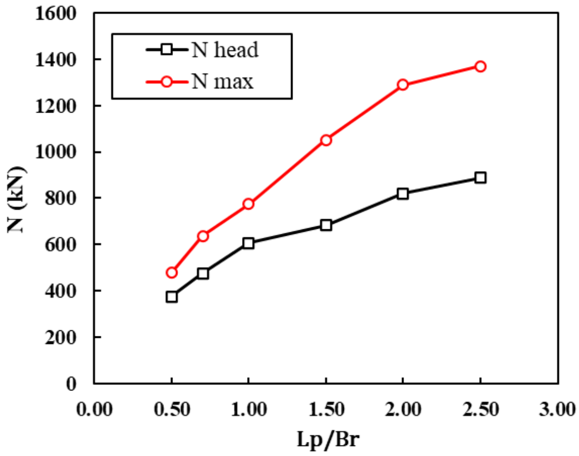


*Fig. 26. Influence of pile length on $N_{head}$ and $N_{max}$ for the middle pile.*

### 3.3.4. BENDING MOMENT DISTRIBUTION ALONG THE PILE

The influence of the $L_p/B_r$ ratio on the bending moment distribution across the length of the middle pile in the DPR system is illustrated in Fig. 27.

It is noted that the bending moment is nearly zero at both ends of the pile, with the maximum bending moment occurring at some depth below the head of the pile, irrespective of the $L_p/B_r$ ratio. Additionally, it is noticed that the maximum bending moment ($M_{max}$) rises, as the $L_p/B_r$ ratio grows.

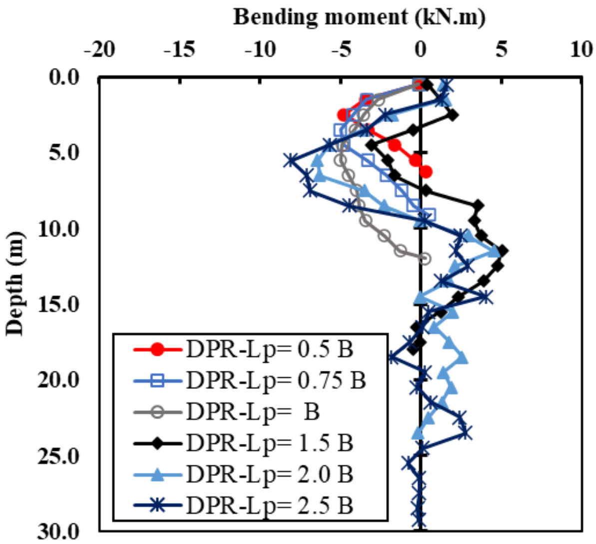


*Fig. 27. Influence of pile length on bending moment distribution along the middle pile.*

The influence of the $L_p/B_r$ ratio on both the $M_{head}$ and the $M_{max}$ is presented in Fig. 28. It is clear that the $L_p/B_r$ ratio has a negligible impact on the $M_{head}$, which tends to stabilize at a value approaching zero. This is because of the cushion layer that separates the piles from the raft, so the pile head is only constrained by the confining stress of the adjacent soil, which is minimal near the ground surface. Conversely, the $M_{max}$ increases with the increases of the $L_p/B_r$ ratio. A sharp rise in the $M_{max}$ is observed when the $L_p/B_r$ ratio surpasses 1.5, i.e., the $M_{max}$ increases by 60.1% as the $L_p/B_r$ ratio rises from 1.5 to 2.5; this significant increase is likely due to the pile beginning to behave as a flexible long pile.

To achieve optimal performance of the studied DPR system, a pile length, with an $L_p/B_r$ ratio of 1.5, is recommended based on the findings in this section.

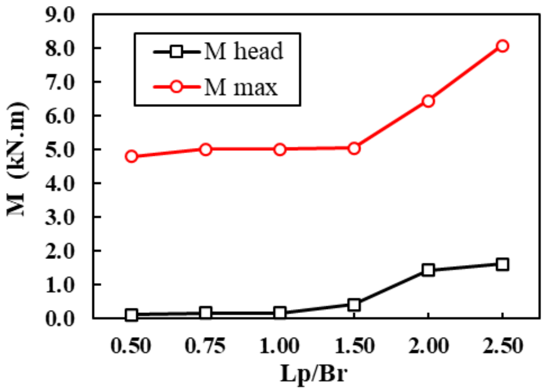


*Fig. 28. Influence of pile length on $M_{head}$ and $M_{max}$ for the middle pile.*

### 3.4. Influence of Pile Diameter on DPR Foundation

Numerical analyses are performed for a square rigid raft of 11.5 m × 11.5 m × 1.5 m supported on 16 disconnected floating piles with constant pile spacing of 3.0 m. All piles have a length ($L_p$) of 17.5 m. The cushion layer has a thickness ($h_c$) of 0.5 m and a Young's modulus ($E_c$) of 48 MPa. The impact of pile diameter ($d_p$) on the performance of the DPR foundation is examined by changing ($d_p$) from 0.3 m to 0.6 m.

#### 3.4.1. Load-Settlement Behavior

Fig. 29 illustrates the load–settlement curves of the DPR for various $d_p$ values. The load–settlement curve of the unpiled raft is also included for reference. It is noted that the raft settlement is significantly reduced to a tolerable level for all the considered DPR foundations. Furthermore, as expected, the settlement of the DPR foundation reduces as the $d_p$ increases. This results from the enhanced stiffness of the pile with an increase in its diameter, thereby improving the load-carrying capacity of both the pile and the DPR system; this behavior aligns with the findings presented in [22].

The effect of $d_p$ on settlement efficiency ($\eta$) at the maximum applied load is presented in Fig. 30. It is evident that increasing $d_p$ enhances the settlement efficiency. The settlement efficiency increases by 10.8%, 8.5%, and 7.8% as $d_p$ increases from 0.3 m to 0.4 m, from 0.4 m to 0.5 m, and from 0.5 m to 0.6 m, respectively.

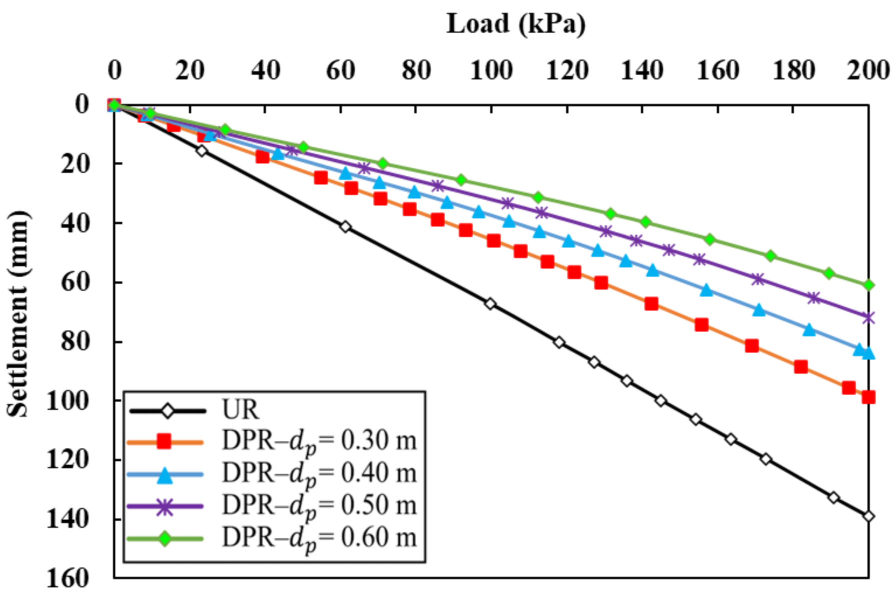


*Fig. 29. Load–settlement curves of the UR, and DPR with different pile diameters.*

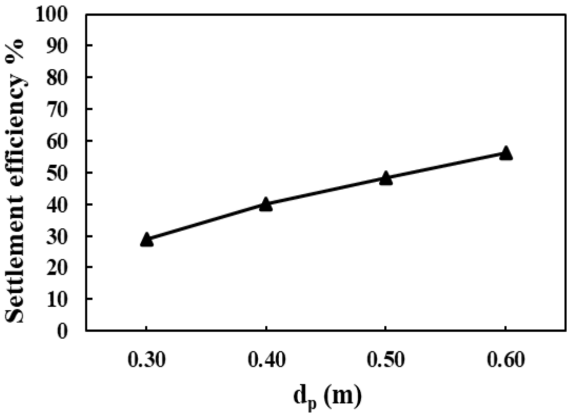


*Fig. 30. Influence of pile diameter ( $d_p$) on settlement efficiency of DPR at a load of 200 kPa.*

### 3.4.2. LOAD SHARING BEHAVIOR

Fig. 31 illustrates how the load sharing between the raft and the piles changes with the pile diameter ($d_p$) at a load of 200 kPa. The findings indicate that the load transferred to the piles rises, and the raft load reduces with the increase in the $d_p$. This is because increasing the pile diameter improves its stiffness, which results in a greater load being transmitted to the piles. For example, as the $d_p$ increases from 0.30 m to 0.60 m, the load taken by the piles increases from 20.6 % to 46.7 %.

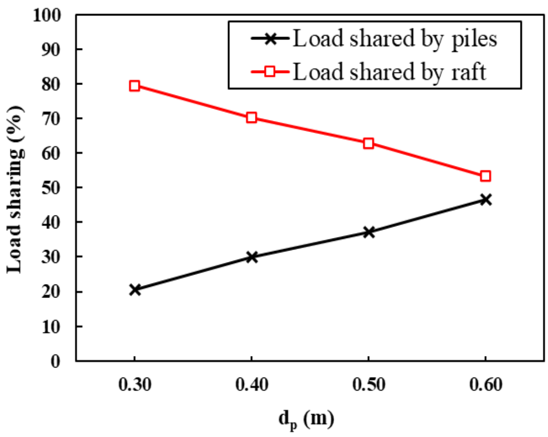


*Fig. 31. Influence of pile diameter ( $d_p$) on the load sharing of DPR at a load of 200 kPa.*

### 3.4. 3. AXIAL LOAD DISTRIBUTION ALONG THE PILE

Fig. 32 demonstrates the impact of $d_p$ on the axial load distribution across the depth of the middle pile in the DPR foundation. The results indicate that as the $d_p$ increases, both the $N_{head}$ and the $N_{max}$ significantly increase. Additionally, the depth of the neutral plane beneath the pile head remains unchanged regardless of the increase in $d_p$. As shown in Fig. 33, $N_{head}$ increases by 47.6%, 20.2%, and 34.5% as $d_p$ increases from 0.3 m to 0.4 m, from 0.4 m to 0.5 m, and from 0.5 m to 0.6 m, respectively. At the same time, $N_{max}$ increases by 40.4 %, 30.5%, and 18.2% over the same intervals of $d_p$.

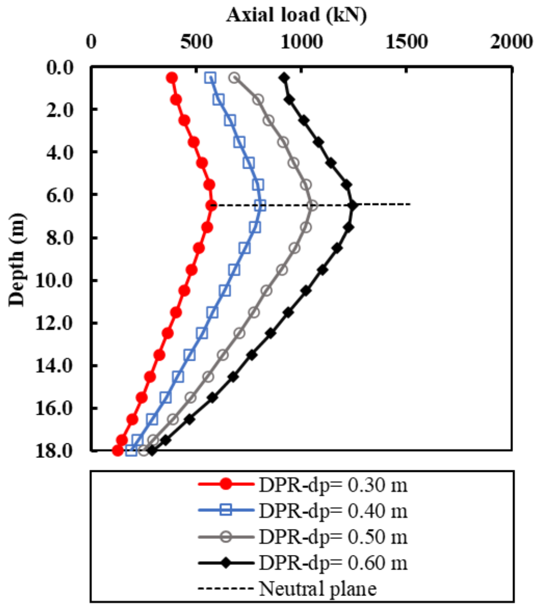


*Fig. 32. Influence of pile diameter on axial load distribution along the middle pile.*

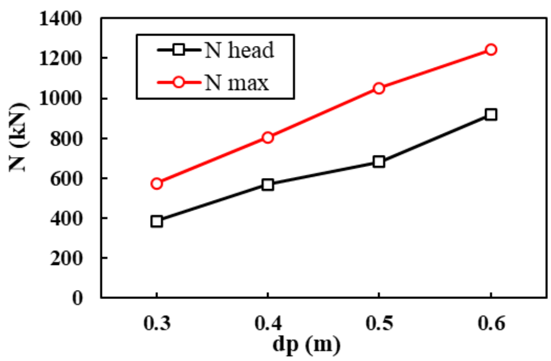


*Fig. 33. Influence of pile diameter ( $d_p$) on $N_{head}$ and $N_{max}$ for the middle pile.*

### 3.4.4. BENDING MOMENT DISTRIBUTION ALONG THE PILE

Fig. 34 illustrates how the pile diameter influences the bending moment distribution across the depth of the middle pile in the DPR foundation. It is noted that the bending moment is almost negligible at both ends of the pile, with the peak bending moment developing at some depth below the pile top, independent of the value of $d_p$. Furthermore, the findings show that the $M_{max}$ increases as the $d_p$ increases. The influence of $d_p$ on both the $M_{head}$ and the $M_{max}$ is presented in Fig. 35. It is evident that the $d_p$ has a negligible impact on the $M_{head}$, which remains nearly constant at a value near zero. This is because of the existence of the cushion layer that disconnects the piles from the raft. As a result, the pile head is mainly restricted by the surrounding soil's confining pressure, which is low near the surface. In contrast, the $M_{max}$ increases with the increases of the $d_p$ (e.g., $M_{max}$ values of 1.77 kN.m, 2.88 kN.m, 5.04 kN.m, and 8.57 kN.m are observed for $d_p$ values of 0.3 m, 0.4 m, 0.5 m, and 0.6 m, respectively).

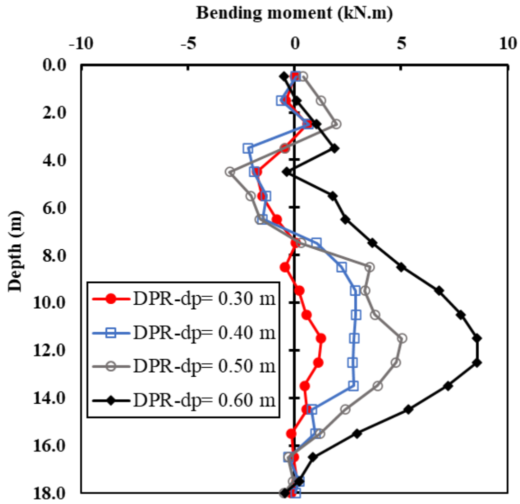


*Fig. 34. Influence of pile diameter on bending moment distribution along the middle pile.*

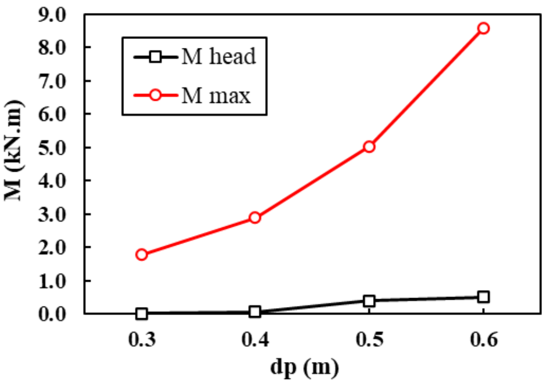


*Fig. 35. Influence of pile diameter (dp) on $M_{head}$ and $M_{max}$ for the middle pile.*

## 4. CONCLUSIONS

A comprehensive parametric study is carried out through the 3D FE method to examine the impact of various efficient factors on the response of the DPR foundation on loose sand under uniform vertical loads. The study explores the effects of the cushion thickness and elasticity modulus, along with the length and diameter of the pile on the load-carrying capacity of the DPR foundation, the distribution of loads among the piles and the raft, and the axial loads and bending moments induced in the floating disconnected piles. The following conclusions can be derived from the parametric study:

1. The performance of the DPR foundation differs significantly from that of the PR foundation, as the granular cushion reduces the stress concentration at pile heads, resulting in a significant reduction in the load transmitted to the piles and more load supported by the shallow subsoil. Furthermore, the existence of the cushion greatly decreases both the axial stress and bending moments at the pile tops. The peak axial load on the disconnected pile is not situated at the top, but at some depth below the pile's top, where the neutral plane exists. This results from the mobilization of negative skin friction across the pile shaft above the neutral plane, caused by the compressibility of the cushion.
2. The granular cushion's thickness significantly influences the behavior of the DPR foundation. Increasing the granular cushion thickness results in less load being transmitted to the piles and more load to the topsoil, thereby increasing the settlement of the DPR system. However, this increase in cushion thickness also reduces both the axial load and bending moments generated in the floating disconnected piles. For optimal performance of the DPR foundation in the studied cases, the cushion thickness should be within the range of 0.5 m to 1.0 m.
3. The elastic modulus of the cushion material, $E_c$, is a key factor influencing the behavior of the DPR system. $E_c$ values should be within the typical range of soil materials. A cushion with an excessively high $E_c$, such as concrete, proves ineffective in optimizing the stress distribution between the piles and the subsoil. In contrast, when the $E_c$ values correspond to typical soil conditions, increasing $E_c$ leads to an increase in the load transmitted to piles and a decrease in the load carried by the underlying soil, which in turn reduces the settlement of the DPR system. However, this increase in $E_c$ also causes higher axial loads and bending moments within the floating disconnected piles. A granular cushion of dense sand, with an elastic modulus of 48 MPa, is suggested to achieve the best performance in the studied DPR systems.
4. Increasing the length of the floating disconnected piles leads to a higher load transmitted to the piles and a reduced load to the topsoil between them, which subsequently decreases the settlement of the DPR system. However, the maximum settlement remains above the allowable limits for $L_p/B_r$ ratios up to 1. Furthermore, longer piles lead to increased axial loads and maximum bending moments

within the piles, which require additional precautions when using long piles in the DPR system. For optimal performance of the DPR systems analyzed, a floating pile with an $L_p/B_r$ ratio of 1.5 is recommended.

5. Increasing the diameter of the floating disconnected piles improves the load-carrying capacity of the individual pile, thereby enhancing the performance of the entire DPR system. Furthermore, both the axial loads and the maximum bending moments within the piles increase as the pile diameter increases.

## ACKNOWLEDGEMENTS

This research is based on the Ph.D. thesis of the second author. The support offered by the Civil Engineering Department at Faculty of Engineering, Menoufia University, Egypt to carry out this study are deeply acknowledged.

## FUNDING

This research has not received any funding from public, commercial, or non-profit organizations.

## CONFLICT OF INTEREST

The authors declare that they have no conflict of interest.

## REFERENCES

[1] R. Banerjee, S. Bandyopadhyay, A. Sengupta, and G. R. Reddy, "Settlement behaviour of a pile raft subjected to vertical loadings in multilayered soil," 2022, *Taylor and Francis Ltd.* doi: 10.1080/17486025.2020.1739754.

[2] P. Halder and B. Manna, "Performance evaluation of piled rafts in sand based on load-sharing mechanism using finite element model," International Journal of Geotechnical Engineering, vol. 16, no. 5, pp. 574–591, 2022, doi: 10.1080/19386362.2020.1729297.

[3] O. A. Abdel-Azim, K. Abdel-Rahman, and Y. M. El-Mossallamy, "Numerical investigation of optimized piled raft foundation for high-rise building in Germany," Innovative Infrastructure Solutions, vol. 5, no. 1, Apr. 2020, doi: 10.1007/s41062-019-0258-4.

[4] A. Z. Elwakil and W. R. Azzam, "Experimental and numerical study of piled raft system," Alexandria Engineering Journal, vol. 55, no. 1, pp. 547–560, Mar. 2016, doi: 10.1016/j.aej.2015.10.001.

[5] A. M. Alnuaim, H. El Naggar, and M. H. El Naggar, "Evaluation of Piled Raft Performance Using a Verified 3D Nonlinear Numerical Model," Geotechnical and Geological Engineering, vol. 35, no. 4, pp. 1831–1845, Aug. 2017, doi: 10.1007/s10706-017-0212-1.

[6] B. El-Garhy, A. A. Galil, A.-F. Youssef, and M. A. Raia, "Behavior of raft on settlement reducing piles: Experimental model study," Journal of Rock Mechanics and Geotechnical Engineering, vol. 5, no. 5, pp. 389–399, 2013.

[7] V. Fioravante, D. Giretti, and M. Jamiolkowski, "Physical modeling of raft on settlement reducing piles," in from research to practice in geotechnical engineering, 2008, pp. 206–229.

[8] L. de Sanctis, A. Mandolini, G. Russo, and C. Viggiani, "Some remarks on the optimum design of piled rafts," in Deep Foundations 2002: An International Perspective on Theory, Design, Construction, and Performance, 2002, pp. 405–425.

[9] H. G. Poulos, "Piled raft foundations: design and applications," Geotechnique, vol. 51, no. 2, pp. 95–113, 2001.

[10] J. B. Burland, "Piles as settlement reducers," The 8th Italian Conference on Soil Mechanics, vol. 2, pp. 21–34, 1995.

[11] M. F. Randolph, "Design methods for pile group and piled rafts," in Proc. 13th Int. Conf. on SFE, 1994, 1994, pp. 61–82.

[12] X. D. Cao, Ing, H. Wong, M. Asce, and M.-F. Chang, "Behavior of Model Rafts Resting on Pile-Reinforced Sand", doi: 10.1061/ASCE1090-02412004130:2129.

[13] A. Taghavi Ghalesari, A. Barari, P. Fardad Amini, and L. B. Ibsen, "Development of optimum design from static response of pile–raft interaction," J Mar Sci Technol, vol. 20, pp. 331–343, 2015.

[14] I. H. Wong, M. F. Chang, and X. D. Cao, "17. Raft foundations with disconnected settlement-reducing piles," Design applications of raft foundations, pp. 469–486, 2000.

[15] A. M. J. Alhassani and A. N. Aljorany, "Experimental and Numerical Modeling of Connected and Disconnected Piled Raft," KSCE Journal of Civil Engineering, vol. 27, no. 6, 2023, doi: 10.1007/s12205-023-0437-x.

[16] Ahmed A. Elsobky, "Numerical Analysis of

Disconnected Piled Raft Foundations," Ph. D. Thesis, Menoufia University, Menoufia, Egypt, 2021.

[17] W. El Kamash, H. El Naggar, M. Nabil, and A. Ata, "Optimizing the Unconnected Piled Raft Foundation for Soft Clay Soils: Numerical Study," KSCE Journal of Civil Engineering, vol. 24, no. 4, 2020, doi: 10.1007/s12205-020-0567-3.

[18] A. Saeedi Azizkandi, H. Rasouli, and M. H. Baziar, "Load Sharing and Carrying Mechanism of Piles in Non-connected Pile Rafts Using a Numerical Approach," International Journal of Civil Engineering, vol. 17, no. 6, 2019, doi: 10.1007/s40999-018-0356-2.

[19] H. Rasouli, A. Taghavi Ghalesari, M. Modarresi , and A. Hasanzadeh, "Numerical Study of Non-Contact Piled Raft Interaction under Static Loads," 2017. doi: 10.1142/9789813225237_0058.

[20] F. Tradigo, F. Pisano, C. di Prisco, and A. Mussi, "Non-linear soil-structure interaction in disconnected piled raft foundations," Comput Geotech, vol. 63, 2015, doi: 10.1016/j.compgeo.2014.08.014.

[21] B. Hor, M. J. Song, M. H. Jung, Y. H. Song, and Y. H. Park, "A 3D FEM analysis on the performance of disconnected piled raft foundation," in 15th Asian Regional Conference on Soil Mechanics and Geotechnical Engineering, ARC 2015: New Innovations and Sustainability, 2015. doi: 10.3208/jgssp.KOR-21.

[22] A. Ata, E. Badrawi, and M. Nabil, "Numerical analysis of unconnected piled raft with cushion," Ain Shams Engineering Journal, vol. 6, no. 2, 2015, doi: 10.1016/j.asej.2014.11.002.

[23] F. Y. Liang, L. Z. Chen, and X. G. Shi, "Numerical analysis of composite piled raft with cushion subjected to vertical load," Comput Geotech, vol. 30, no. 6, 2003, doi: 10.1016/S0266-352X(03)00057-0.

[24] H. J. Park et al., "Centrifuge modeling of disconnected piled raft using vertical pushover tests," Acta Geotech, vol. 15, no. 9, 2020, doi: 10.1007/s11440-020-00928-6.

[25] V. Fioravante and D. Giretti, "Contact versus noncontact piled raft foundations," Canadian Geotechnical Journal, vol. 47, no. 11, 2010, doi: 10.1139/T10-021.

[26] M. El Sawwaf, "Experimental study of eccentrically loaded raft with connected and unconnected short piles," Journal of geotechnical and geoenvironmental engineering, vol. 136, no. 10, pp. 1394–1402, 2010.

[27] X. Zhu, "Analysis of the load sharing behaviour and cushion failure mode for a disconnected piled raft," Advances in Materials Science and Engineering, vol. 2017, no. 1, p. 3856864, 2017.

[28] M. Ghanbar Dezfouli, M. Dehghani, A. Asakereh, and B. Kalantari, "Behavior of geogrid reinforced and unreinforced non-connected pile raft foundation," International Journal of Civil Engineering, vol. 17, pp. 709–722, 2019.

[29] A. Saeedi Azizkandi and R. Taherkhani, "Experimental study on connected and non-connected piled raft foundations subjected to eccentric loading," International Journal of Civil Engineering, vol. 18, pp. 743–761, 2020.

[30] P. Halder and B. Manna, "Load transfer mechanism for connected and disconnected piled raft: a comparative study," Acta Geotech, vol. 17, no. 7, pp. 3033–3045, 2022.

[31] P. Halder and B. Manna, "Large scale model testing to investigate the influence of granular cushion layer on the performance of disconnected piled raft system," Acta Geotech, vol. 16, no. 5, pp. 1597–1614, 2021.

[32] R. Brinkgreve and P. A. Vermeer, "PLAXIS 3D reference manual CONNECT edition V20," Delft University: Delft, The Netherlands, 2019.

[33] M. H. Zakaria and A. Basha, "Two-Dimensional Numerical Approaches of Excavation Support Systems: A Comprehensive Review of Key Considerations and Modelling Techniques," Journal of Contemporary Technology and Applied Engineering, vol. 3, no. 1, pp. 64–74, 2024.

[34] R. B. J. Brinkgreve, E. Engin, and H. K. Engin, "Validation of empirical formulas to derive model parameters for sands," in Numerical Methods in Geotechnical Engineering - Proceedings of the 7th European Conference on Numerical Methods in Geotechnical Engineering, 2010. doi: 10.1201/b10551-27.

[35] D. Park, D. Park, and J. Lee, "Analyzing load response and load sharing behavior of piled rafts installed with driven piles in sands," Comput Geotech, vol. 78, 2016, doi: 10.1016/j.compgeo.2016.05.008.